ELSEVIER

Contents lists available at ScienceDirect

Chemical Engineering Journal

journal homepage: www.elsevier.com/locate/cej





Improving UV protection and retention of photosensitive agrochemicals: Innovative polyurethane-CeO₂ hybrid pesticide microcapsules

Nianlei Zhang ^{a,1}, Yanan Xiao ^{a,1}, Shuhui Hu ^{b,1}, Qian Chen ^a, Yan Huang ^a, Mengdie Li ^a, Zijing Jin ^a, Huaixiang Chen ^c, Wenneng Wu ^{b,*}, Jian Wang ^{a,*}, Bo Zhang ^{a,*}

- ^a Shanghai Engineering Research Center of Green Energy Chemical Engineering, The Key Laboratory of Resource Chemistry of Ministry of Education, College of Chemistry and Materials Science, Shanghai Normal University, 100 Guilin Road, Shanghai 200234, PR China
- Food and Pharmaceutical Engineering Institute, Guiyang University, Guiyang 550003, PR China

ARTICLE INFO

Keywords:
Photosensitive pesticide
UV stability
Foliar retention
Polyurethane microcapsule
CeO₂ nanoparticles
Pyraclostrobin

ABSTRACT

Photolysis and poor retention significantly decrease the utilization efficiency of photosensitive agrochemicals, leading to considerable ecological and economic losses. We successfully prepared novel pyraclostrobin-loaded polyurethane-inorganic hybrid microcapsules (Pyr@KCeO2-PU MCs) with high adhesion and UV stability by interfacial polymerization. CeO2 nanoparticles (NPs) were incorporated as UV light absorbers, while a silane coupling agent (KH550) was employed for in situ crosslinking of PU with CeO₂ NPs, facilitating their dispersion within the PU shell. Characterization results revealed a high encapsulation efficiency of 90 % and uniform sizes (D₅₀ = 915 nm) for the Pyr@KCeO₂-PU MCs. Optical property investigations using UV-vis spectroscopy indicated that the integration of CeO2 NPs within the PU shell produced stronger UV absorption bands compared to both Pyr technical (TC) and Pyr@PU MCs. This observation underscores the potential of CeO2 NPs as effective UV absorbers. The anti-photolysis performance of Pyr@KCeO₂-PU MCs improved with the addition of CeO₂ NPs, yielding a retention rate of Pyr in Pyr@KCeO2-PU MCs that was 1.90 and 1.27 times greater than that of Pyr TC and Pyr@PU MCs, respectively, under UV irradiation. Furthermore, KH550 not only facilitated crosslinking between PU and CeO2 NPs, ensuring uniform distribution of CeO2 NPs on the PU shell surface, but also enhanced wettability and foliar retention. The contact angle of Pyr@KCeO2-PU MCs (32°) was significantly lower than that of Pyr@PU MCs (84°), and Pyr retention on rice leaves was 17.5 mg/cm² for Pyr@KCeO₂-PU MCs, surpassing that of Pyr@PU MCs (9.3 mg/cm²). Additionally, Pyr@KCeO₂-PU MCs exhibited superior efficacy against various plant pathogens compared to Pyr TC and Seltima. These findings highlight the potential of Pyr@KCeO2-PU MCs for enhancing pesticide utilization and offer valuable insights for the future development of PU-based pesticide formulations.

1. Introduction

The widespread application of pesticides is crucial for enhancing both the yield and quality of crop production [1]. However, conventional pesticide formulations often suffer significant losses to the environment due to factors such as spray drift, rainwater runoff, poor wettability, inadequate adhesion, and photodecomposition during application. Consequently, the effective utilization of pesticides can be less than 0.1 % [2]. Notably, certain photosensitive pesticides

experience approximately 50 % loss during application due to photolysis, which further diminishes their efficacy [3]. Various strategies have been proposed to improve the photostability of pesticides, including the incorporation of light stabilizers [4], anti-photolysis carrier materials [5], and microencapsulation [6]. Among these, microencapsulation technology has demonstrated considerable promise in mitigating pesticide photolysis and is relatively straightforward to implement. Microcapsules (MCs) composed of various wall materials have been employed to shield pesticides from UV degradation [6–10]. Additionally, the

^c ADAMA Huifeng (Jiangsu) Ltd., PR China

^{*} Corresponding authors at: Shanghai Engineering Research Center of Green Energy Chemical Engineering, The Key Laboratory of Resource Chemistry of Ministry of Education, College of Chemistry and Materials Science, Shanghai Normal University, 100 Guilin Road, Shanghai 200234, PR China.

E-mail addresses: wennengwu123@126.com (W. Wu), jianwang@shnu.edu.cn (J. Wang), zb830216@shnu.edu.cn (B. Zhang).

 $^{^{1}\,}$ These authors contributed equally.

design and materials of the MC shell are pivotal to their performance. Exploring different shell configurations to enhance foliar retention, such as through surface modification and flexible shells, constitutes a significant research avenue [11,12]. Thus, the advancement of pesticide microencapsulation systems presents substantial potential for achieving high encapsulation efficiency of active ingredients, improving foliar affinity, and enhancing anti-UV performance. This, in turn, could lead to reduced foliar pesticide loss, increased resistance to UV degradation, and diminished environmental risks.

Among the various microencapsulation methods, interfacial polymerization is the most widely utilized technique for encapsulating agrochemicals, attributed to its simplicity, cost-effectiveness, rapid reaction rate, high encapsulation efficiency, and suitability for continuous production [13–15]. Polyurethane or polyurea (PU) is the predominant shell material employed in interfacial polymerization, owing to its compatibility, durability, and favorable mechanical properties [9,12–16]. Notably, PU-based hybrid microcapsules (MCs) have been recognized for their significant role in specialized applications, as they provide a platform for integrating multiple complementary components through decoration or functionalization into a single functional system. This capability not only protects active ingredients from harsh environments but also allows for the modulation of drug release rates, enhanced resistance to photolysis, and improved adhesion to foliage [17–20].

Various inorganic nanoparticles (NPs), such as TiO_2 , CeO_2 , and ZnO, have been recognized as effective agents for UV shielding [21–23]. Among these, CeO_2 NPs demonstrate superior UV absorption capabilities compared to both TiO_2 and ZnO. This enhanced performance is attributed to the relatively small band gap of CeO_2 , which is 3.1 eV, lower than that of TiO_2 (3.27 eV) and ZnO (3.37 eV). The reduced band gap facilitates the transition of valence electrons in CeO_2 , thereby enhancing its applicability in UV shielding applications [24]. Furthermore, incorporatiing CeO_2 into polyurethane to create hybrid nanocomposites has been shown to significantly improve the UV-shielding effectiveness of polyurethane [25–27].

Pyraclostrobin (Pyr) is extensively utilized for the control of various fungal diseases, due to its high potency, broad spectrum of activity, and low toxicity to mammals [28]. However, the rapid photolysis of Pyr, with a degradation half-life (DT₅₀) as short as 39 min under ultraviolet light, poses challenges in effectively preventing the onset and spread of fungal diseases over prolonged periods [29]. To address this issue, the type of polyamines is demonstrated to significantly influence the physicochemical properties of PU-MCs. Cao et al. reported that Pyr-loaded PU-MCs were fabricated with different polyamines as cross-linkers, and the UV resistance of the shells was observed with incrrasing carbon skeleton of polyamines [15]. In this study, we developed a PUinorganic hybrid shell that incorporates functionalized CeO2 NPs with UV-shielding capabilities. Pyr@KCeO2-PU MCs were successfully fabricated through interfacial polymerization, which involved a systematic polyaddition process at the O/W interface of droplets. Prior to application, the CeO2 NPs were functionalized through a reaction with KH550, which introduced -NH2 moieties onto the NP surface (Fig. S1, Fig. S2, and Table S2). The highly reactive –NH₂ groups at the terminal ends of the KH550 molecular chains facilitate interaction with the isocyanate groups in PU (Scheme 1). This functionalization significantly enhanced the crosslinking between PU and CeO2 NPs while also improving the dispersion of the CeO2 NPs within the composite shell. Furthermore, it increased the wettability and foliar retention of the Pyr@KCeO2-PU.

MCs on leaf surfaces. We conducted a comprehensive investigation into the morphology, structure, particle size, sustained release behavior, foliar wetting and adhesion performance, rain washout resistance, and antifungal activity of the Pyr@KCeO₂-PU MCs. Additionally, we assessed antifungal activities and cytotoxicity to evaluate the potential application of these hybrid MCs. This research amis to provide novel insights into the preparation of multifunctional pesticide microcapsules

and to enhance the efficient utilization of pesticides.

2. Experimental

2.1. Materials

Isophorone diisocyanate (IPDI), polyethylene glycol 600 (PEG 600), dibutyltin dilaurate (DBTDL), triethylenetetramine (TETA), polyoxyethylene castor oil (EL-40), trimethylamine (TEA), butane-1,4-diol (BDO), aromatic solvent oil (S-150), KH-550 and CeO2 with a particle size of 20-30 nm were analytical reagent and purchased from Shanghai Titan Scientific Co., Ltd. (Shanghai, China). Deionized water was prepared in the laboratory. Pyr TC (purity 98 %) was supplied by the Hubei Jiu Feng Long Chemical Co., Ltd.. A commercial Pyr MC suspension (Seltima, 9 % CS) was bought from BASF SE (Ludwigshafen, Germany). Tested strains (Rice Blast Fungus, Botrytis cinerea, Rice sheath blight pathogen, Colletotrichum gloeosporioides, Tobacco grey mould, Sclerotinia sclerotiorum) were provided by the School of Food Science and Engineering, Guiyang University. Potato dextrose agar medium (PDA) was prepared using a formula consisting of 200 g potato, 20 g glucose, 15 g agar powder, and pure water to make up to 1 L. The medium was sterilized under high temperature and pressure at 121 °C for 30 min and was utilized for assessing the drug efficacy of the sample. All chemicals were used without further purification.

2.2. Preparation of KH550-CeO₂ (KCeO₂), blank PU MCs, KCeO₂@PU MCs, Pyr@PU MCs and Pyr@KCeO₂-PU MCs

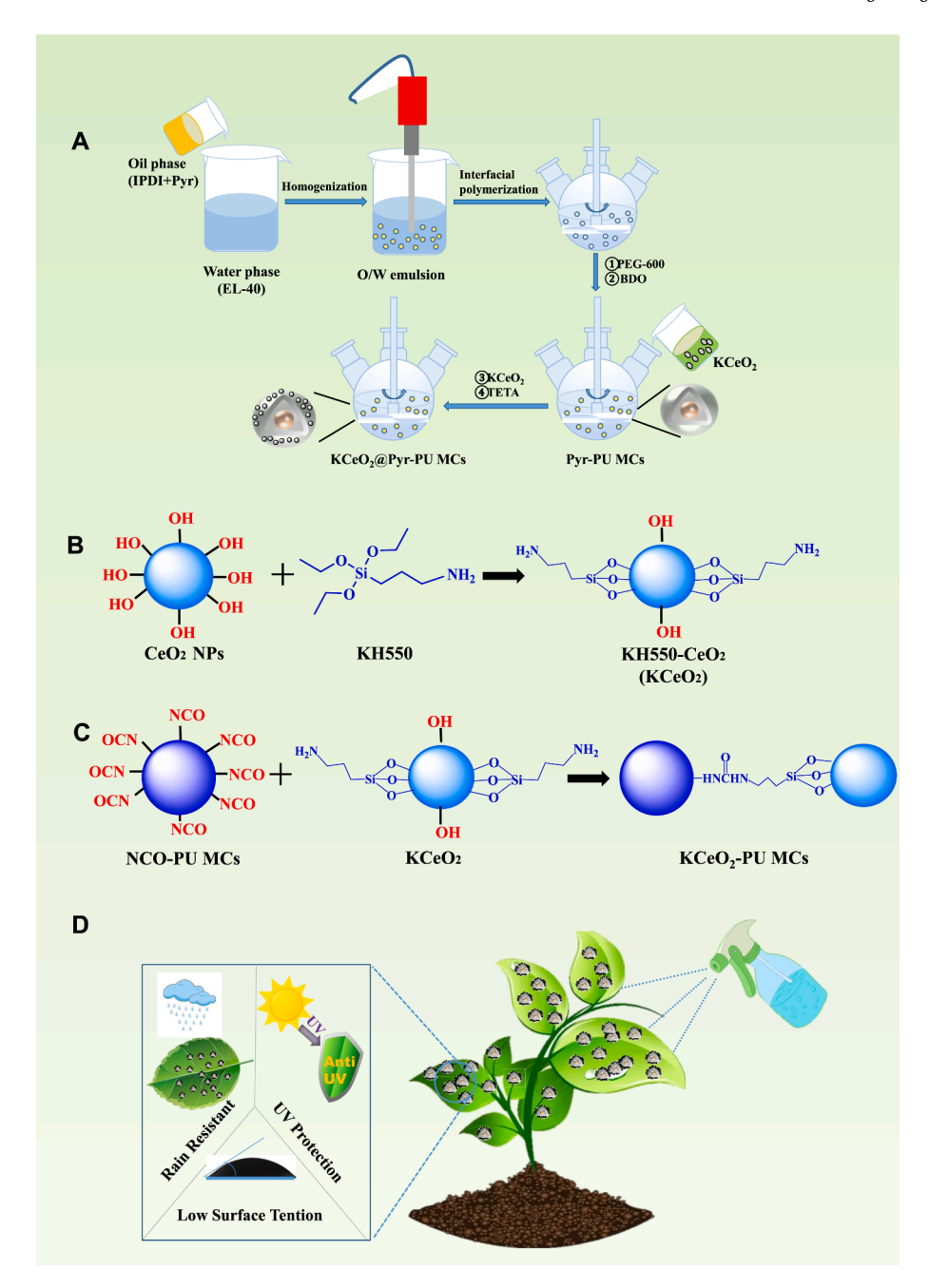
2.2.1. Modification of CeO₂ NPs with KH550 (KCeO₂)

KH550 was chemically grafted onto CeO_2 NPs to produce KCeO₂, following a procedure previously documented in the literature [30]. Typically, 1 g of dried CeO_2 NPs was dispersed in 100 mL of anhydrous ethanol, and 0.1 g of KH550 was slowly added to the suspension while adjusting the pH to 6 with TEA. The reaction mixture was then refluxed and vigorously stirred for 5 h. The resulting products were washed with absolute ethanol and deionized water multiple times, followed by drying overnight in a vacuum oven at 60 °C. The synthesis pathway for CeO_2 NPs functionalized with alkoxysilane groups is visually depicted in Scheme 1B.

2.2.2. Fabrication of Pyr@KCeO2-PU MCs

Pyr@KCeO2-PU MCs were synthesized following the method outlined in Scheme 1C, with modifications as documented previously [31]. Initially, EL-40 (2 g) was dissolved in 100 g of deionized water, which was then divided into two equal parts. Subsequently, KCeO2 (0.1 g) was suspended in 50 mL of the solution and subjected to ultrasonic treatment for 20 min to achieve a homogeneous suspension. The remaining 50 mL of the solution served as the water phase. In parallel, Pyr (6 g) and IPDI (3.6 g) were dissolved in an organic solvent S-150 to form the organic phase. The organic phase was then added dropwise into the water phase under high shear at 10000 rpm for 5 min to create a stable oil-in-water (O/W) emulsion at room temperature. This emulsion was promptly transferred to a three-necked flask and subjected to mechanical stirring at 300 rpm. Subsequently, PEG 600 (2 g) was slowly added dropwise to the O/W emulsion. The polymerization reaction was carried out at 60 $^{\circ}$ C for 1 h, followed by the addition of BDO (0.9 g) and further reaction for 1 h at the same temperature. The KCeO₂ suspension was then gradually introduced to the emulsion and allowed to react for 1 h. Finally, the aqueous solution of TETA (10 g) was slowly added to the system and stirred for 1 h at 60 $^{\circ}$ C. Upon completion of the reaction, the product was obtained. Finally, the Pyr@KCeO2-PU MCs were obtained with Pyr constituting approximately 4.5 % by weight.

The preparation process for the other MCs as control samples closely mirrored that of the Pyr@KCeO₂-PU MCs. In the case of the blank PU MCs, the oil phase was comprised solely of solvent oil, and the aqueous phase did not contain KCeO₂. Conversely, for the KCeO₂-PU MCs, the oil



Scheme 1. Synthetic processes of Pyr@KCeO₂-PU MCs A) and their application D). B) Schematic illustration of the synthesis of KCeO₂. C) Process for the preparation of KCeO₂-PU MCs.

phase also consisted exclusively of solvent oil, whereas the Pyr@PU MCs were characterized by the absence of KCeO $_2$ in the aqueous phase.

2.3. Characterization

The morphology and elemental composition of the samples were analyzed using a scanning electron microscope (FESEM, S-4800, Hitachi Ltd., Tokyo, Japan) equipped with an energy-dispersive spectrometer (EDS). Average particle sizes were determined using a Malvern Zetasizer Nano-ZS instrument (ZS90, Malvern Panalytical Co., Ltd., England) at room temperature after diluting the samples 100 times with deionized water. Fourier transform infrared (FT-IR, Thermo Scientific Nicolet 6700) spectra were recorded with a spectrometer in the wavelength range of 400–4000 cm⁻¹. Thermogravimetric analysis (TGA) was carried out on a thermal analyzer (NETZSCH STA 449F5, NETZSCH Group,

Germany) with a heating rate of 10 K/min from 30 to 600 $^{\circ}$ C under a nitrogen flow of 50 mL/min. Fluorescence imaging of leaves was conducted using a laser confocal microscope (Carl Zeiss LSM DuoScan). The rheological properties of the samples are measured on the rotational rheometer (Anton Paar (Shanghai) Trading Co., Ltd.) [35]. The samples were measured at 25 $^{\circ}$ C.

2.4. Drug-loading capacity (LC) and encapsulation efficiency (EE) of the $Pyr@KCeO_2-PU$ MCs

Drug-loading capacity (LC) and encapsulation efficiency (EE) of the $Pyr@KCeO_2-PU$ MCs were determined as follows: 0.010 g of $Pyr@K-CeO_2-PU$ MCs (with an accuracy of 0.001 g) was mixed with 100 mL of methanol solution and the absorbance was measured using a UV spectrophotometer. The mixture was then sonicated for 30 min and

centrifuged before measuring the absorbance again. The concentration of active ingredients released from the MCs was determined using a standard curve method. The LC (%) and EE (%) of the MCs were then calculated.

$$LC(\%) = \frac{weight \, of \, Pyr \, encapsulated \, in \, microcapsules}{weight \, of \, microcapsules} \times 100$$

$$EE(\%) = \frac{\text{weight of Pyr encapsulated in microcapsules}}{\text{initial weight of Pyr employed}} \times 100$$

2.5. Release behavior

The release performance of Pyr@KCeO2-PU MCs was investigated using a dynamic dialysis method [32]. In this procedure, Pyr@KCeO₂-PU MCs were dispersed in 3 mL of methanol within a dialysis membrane, which was subsequently sealed into a 250 mL beaker containing 197 mL of methanol. The beaker was placed in a steam bath constanttemperature oscillator (THZ-82, Changzhou Yineng Experimental Equipment, JiangSu, China) and shaken at 105 rpm at 25 °C. At specified time intervals, 3 mL aliquots of the solution outside the dialysis membrane were collected and replaced with an equal volume of fresh solution. The sustained release properties of Pyr@KCeO2-PU MCs were evaluated by measuring the concentrations of Pyr dissolved in the release medium at various intervals. The concentration of Pyr was determined using a UV-vis spectrophotometer at 274 nm. The release performance of Pyr@PU MCs exhibited behavior similar to that of Pyr@KCeO2-PU MCs. The cumulative release rate of Pyr was calculated using the provided formula.

$$Q = \frac{CnV + Vi\sum_{i}^{n-i}Ci}{m} \ \times 100$$

where Q is the cumulative release (%) of Pyr, Cn is the Pyr concentration in the release medium at time n, V is the volume of release solution (200 mL), Vi is the volume of the sample taken at a given time interval (Vi = 3 mL), and m is the total amount of pesticide encapsulated in the microcapsules.

2.6. Photostability performance

200~mL of methanolic dispersions of the same concentration of Pyr were prepared. These suspensions were stirred magnetically at 50~r/ min, and maintained at 25 ± 2 °C. They were then irradiated under a UV lamp (36 W, 254 nm) at airtight intervals. Samples were taken at regular intervals and the absorbance was measured at 274 nm using a UV spectrophotometer. The MC suspensions were disrupted by sonication prior to measurement, and the remaining Pyr content was determined based on the absorbance values [9]. Additionally, the UV–Vis spectrum of Pyr@KCeO2-PU MCs, Pyr@PU MCs, and Pyr TC was measured in the wavelength range of $200{-}800~nm$.

The degradation mechanism of Pyr formulations was studied by employing a pseudo-first-order kinetic model (Equation (1), and Equation (2) was used to calculate the half-life $(t_{1/2})$ time of the formulations.

$$y = exp^{-kt}$$

$$t_{1/2} = \frac{ln2}{k}$$

where, t is the radiation time and k is the rate constant.

2.7. Contact angle test

The wettabilities of Pyr@PU MCs and Pyr@KCeO₂-PU MCs solutions on rice leaves were investigated by measuring contact angles [33]. Fresh rice leaves from the laboratory were cleaned, dried, and then fixed onto

glass slides. The 1 mL of 4.5 % Pyr@PU MCs and Pyr@KCeO $_2$ -PU MCs suspensions were diluted 100 times with water. Subsequently, 2 μL of suspension was carefully dropped on the leaves using a microsyringe. Images of the liquid drops were captured and the corresponding contact angles at various time points were measured using a contact angle meter (DSA 30; KRUSS, Germany). Contact angle values were determined using protractor software. Each sample was tested in triplicate at a minimum.

2.8. Adhesion test of Pyr@KCeO2-PU MCs and Pyr@PU MCs

An adhesion test for the samples was undertaken using a previously reported method [34]. Briefly, freshly cleaned rice leaves were cut into strips measuring 1 cm \times 6 cm, with the total area denoted as S cm². Then the leaves were dipped vertically into tenfold diluted Pyr@KCeO2-PU MCs and Pyr@PU MCs solutions for 30 s. Subsequently, each leaf was placed on an analytical balance both before and after soaking to determine the mass difference (Wg) of each leaf. The liquid holding capacity (LHC) was calculated using the following formula:

$$LHC(mg/cm^2) = \frac{1000 \times Wg}{S}$$

To further assess the retention property of the samples on the leaves, a simulated rainwater scour experiment was conducted by UV–vis absorption and fluorescence observation method. For UV–vis absorption, the samples with the equal amount of Pyr were uniformly spread onto at the same size of rice leaves. After natural drying, the leaves were cut into small pieces, and leaves were divided into two groups, each containing pieces of leaves measuring 1 cm \times 3 cm. A group of leaves without being rinsed with water served as a control, whereas the leaves in the experimental group were gently rinsed with 10 mL of distilled water at a 60° angle to mimic rain. Subsequently, two groups of leaves were immersed in 100 ml of methanol solution to clean the residual Pyr by ultrasonic waves. The amount of remaining Pyr was determined with a UV–vis. Each sample was tested three times.

For fluorescence observation, 0.5 mL of the retention of Pyr@KCeO $_2$ -PU MCs was also observed using a fluorescence microscope by spraying its suspension of Pyr@KCeO $_2$ -PU MCs onto rice leaves. The leaves were then placed on a glass plate and dried at room temperature. Fluorescence microscopy ($\lambda ex=550$ nm) was used to image the leaves. Afterwards, the leaves were rinsed with deionized water at a 60° angle for 1 min and reimaged with a fluorescence microscope ($\lambda ex=550$ nm).

2.9. Antifungal activity assays of Pyr@KCeO2-PU MCs

The in vitro antibacterial activity of Pyr@KCeO2-PU MCs against *rice blast fungus, cucumber cinerea, rice sheath blight, anthracnose, soot,* and *Sclerotinia sclerotiorum* was assessed using the mycelial growth inhibition method [36]. Specifically, 0.222 g of Pyr@KCeO2-PU MCs (4.5 % Pyr), 0.111 g of commercial Seltima (9 % Pyr), 0.010 g of Pyr TC, and 0.040 g of blank PU MCs (100 %) were weighed and dissolved in 0.3 mL of DMSO to create a mother solution with a mass concentration of 2000 μ g/mL. This solution was then added to the PDA medium to create a drug-containing medium. The mass concentration of Pyr was 1 μ g/mL, and the mass concentration of blank PU MCs was 500 μ g/mL. PDA treated with only DMSO served as a blank control. A fungus cake with a diameter of 5.00 mm was taken, and a mycelium plug was placed in the center of each culture medium. The medium was then incubated at (25

 \pm 2) °C for 5–6 days, and the radial growth of hyphae was measured. This experiment was repeated three times, and the antibacterial rate was calculated using a specific formula (1):

$$Inhibition(\%) = \frac{\textit{OD}_{colony\,diameter\,of\,control}\ - \textit{OD}_{colony\,diameter\,of\,treatment}}{\textit{OD}_{colony\,diameter\,of\,control}\ - \textit{OD}_{diameter\,of\,mycelial\,discs}} \times 100\%$$

(1)

2.10. Cytotoxicity

2.10.1. Cell culturing

LO2 human liver cell line was obtained from East China University of Science and Technology. The cells were cultured in RPMI-1640 modified liquid medium containing 10 % fetal bovine serum and 1 % double antibodies (100 $\mu g\ mL^{-1}$ penicillin and 100 μ mL $^{-1}$ streptomycin) at 37 °C with 5 % CO2.

2.10.2. Cell viability assay

The impact of Pyr TC, and Pyr@KCeO2-PU MCs on the viability of LO2 hepatocytes was evaluated through the CCK-8 method. Once the cells reached the logarithmic growth phase, they were harvested, resuspended in fresh culture medium, and inoculated into 96-well plates at 100 μL per well. Subsequently, the cells were exposed to 0.01–0.05 mg/L of Pyr TC, Seltima and Pyr@KCeO2-PU MCs, follow by an incubation period in a 5 % CO2 incubator at 37 °C. The control group consisted of LO2 cells and culture medium without any drug, while the blank group contained only the culture medium. Each treatment was conducted in triplicate. 10 μL of CCK-8 was added to each well and incubated in the incubator at 37 °C for 2 h. Absorbance at 450 nm (optical density, OD) was measured with enzyme markers, and the formula for calculating cell viability was as follows.

$$Cell\ viability = rac{OD_{treatment\ group} - OD_{blank\ group}}{OD_{control\ group} - OD_{blank\ group}} imes 100\%$$

3. Results and discussion

3.1. Preparation and characterization

Pyr@KCeO₂-PU MCs were successfully fabricated through interfacial polymerization, as illustrated in Scheme 1A and Scheme S1. Initially, an O/W emulsion was created by homogenizing Pyr TC and IPDI butyl

acetate solutions with an aqueous phase containing emulsifiers (EL-40). Isocyanate-terminated prepolymer microcapsules with urethane linkages were then synthesized via primary interfacial polymerization of IPDI and PEG-600, while encapsulating Pyr. Subsequently, BDO was introduced as a chain extender to react with the isocyanate groups in the prepolymer, leading to the formation of long chain linear block copolymers. Then, the addition of KCeO₂ in the aqueous phase further enhanced the shell. KCeO₂, containing numerous highly active amino groups, easily undergoes chemical reactions with isocyanate group in isocyanate-terminated prepolymer under mild conditions, facilitating further surface modification of MCs. The final step involved adding polyamine TETA as a curing agent to increase cross-link density, resulting in thicker and stronger microcapsule shells. Ultimately, Pyr@KCeO₂-PU MCs were successfully synthesized.

FESEM was employed to characterize the morphologies of the samples, as depicted in Fig. 1A-C. The Pyr@KCeO2-PU MCs displayed a spherical morphology with an average diameter of 915 nm (Fig. 1E). The outer surface of the MCs appeared coarse, possibly attributed to the random deposition of CeO_2 NPs (Fig. 1C), resulting in a rough surface with protruding nubs-like structures (Fig. 1B). EDS data (Fig. 1D) confirmed the presence of Ce element with a weight percentage of 0.08 % (Table S1) on the surface of the Pyr@KCeO2-PU MCs, indicating successful deposition of CeO_2 on PU shell. DLS measurements revealed that the Pyr@KCeO2-PU MCs had a larger particle size compared to Pyr@PU MCs, providing further evidence of the successful deposition of CeO_2 on the MCs surface.

3.2. Chemical component analysis of the samples.

Fig. 2A illustrated the FTIR spectra of Pyr TC, blank PU MCs, and Pyr@KCeO₂-PU MCs, respectively. The intense absorption peak at $1717.78~{\rm cm}^{-1}$ corresponds to the C = O stretching vibration of Pyr TC. The absence of characteristic peaks associated with isocyanate groups in the blank PU MCs indicates that a crosslinking reaction has occurred

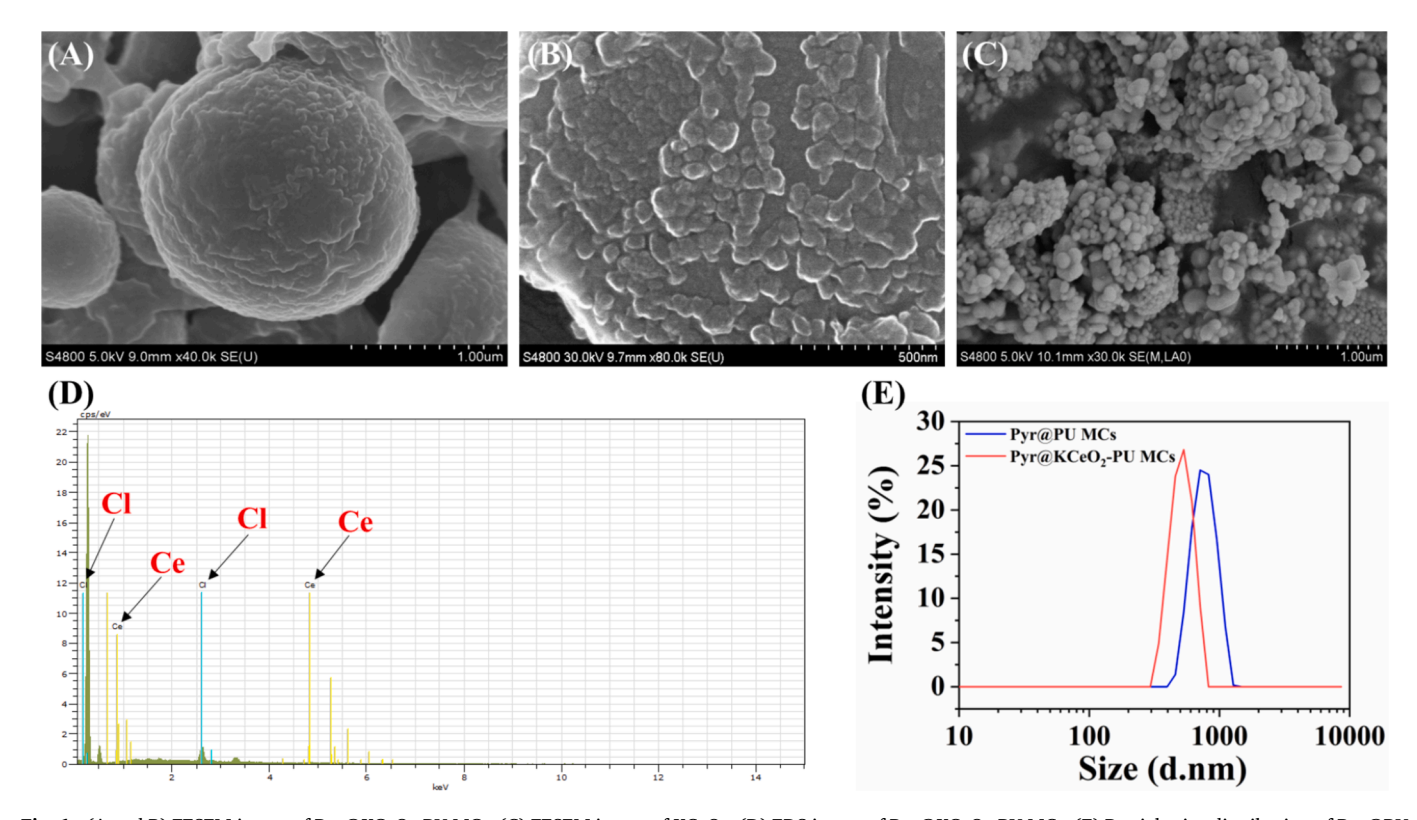


Fig. 1. (A and B) FESEM image of Pyr@KCeO₂-PU MCs; (C) FESEM image of KCeO₂; (D) EDS image of Pyr@KCeO₂-PU MCs; (E) Particle size distribution of Pyr@PU MCs (blue line) and Pyr@KCeO₂-PU MCs (red line).

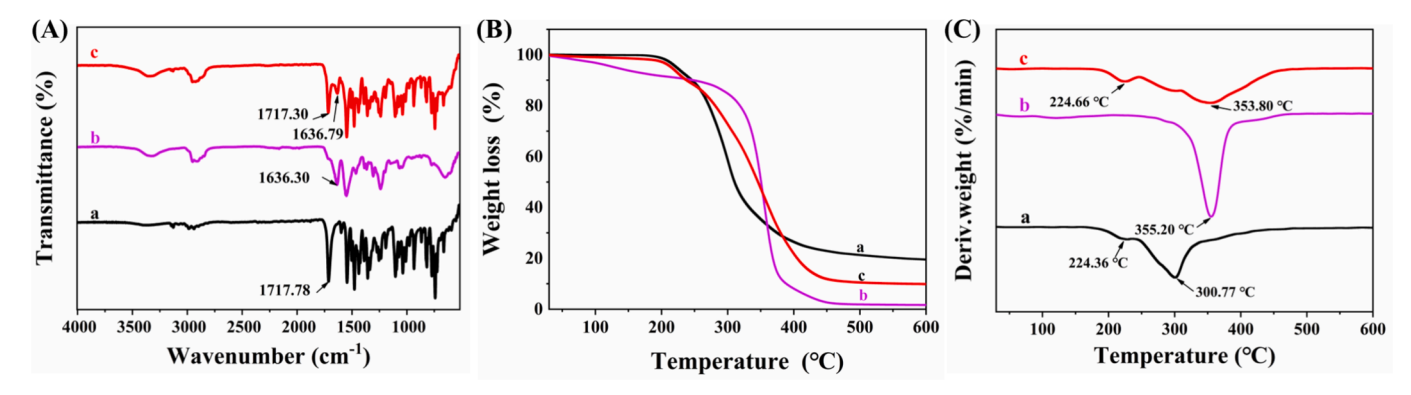


Fig. 2. (A) FTIR spectra, (B) TGA and (C) DTG spectrogram diagram of (a) Pyr TC, (b) blank PU MCs and (c) Pyr@KCeO2-PU MCs.

[37]. A peak observed at $1636.30~{\rm cm}^{-1}$ corresponds to the C = O stretching vibration of the polyurethane shell. A comparison of the FTIR spectra of Pyr@KCeO2-PU MCs with those of Pyr and blank PU MCs demonstrates the presence of characteristic absorption peaks of Pyr; however, the characteristic peak of –NCO at 2254.87 cm $^{-1}$ is absent, signifying the formation of the PU shell. Furthermore, the absence of new peaks confirms the successful encapsulation of Pyr within the Pyr@KCeO2-PU MCs.

3.3. Thermal stability analysis

TGA and DTG (Fig. 2B and C) were conducted to assess the thermal stability of Pyr, blank PU MCs, and Pyr@KCeO2-PU MCs. The analyses revealed a progressive weight loss as the temperature increased. Pyr exhibited a single-stage weight loss occurring between 200 °C and 550 °C, which was attributed to decomposition (Fig. 2B, curve a), consistent with previous studies [38]. In contrast, blank PU MCs demonstrated a three-stage weight loss pattern (Fig. 2B, curve b): water evaporation below 100 °C, decomposition of urethane and soft segments from 224 °C to 300 °C, and subsequent fracture of hard segments. Pyr@KCeO2-PU MCs showed weight loss predominantly in the range of 220 °C to 300 °C, attributed to the volatilization of Pyr and the decomposition of carbamate bonds (Fig. 2B, curve c). These findings confirm that Pyr was effectively encapsulated within the MCs shell. The DTG analysis (Fig. 2C) indicated that Pyr@KCeO2-PU MCs exhibited a higher initial decomposition temperature and a reduced weight loss rate compared to Pyr, suggesting that the encapsulation process significantly enhances the thermal stability of Pyr.

3.4. Release profile of MCs

Conventional pesticide formulations, such as emulsifiable concentrates (EC), often encounter challenges related to the rapid release of active ingredients, resulting in diminished effectiveness and increased pesticide usage. In contrast, the controlled release of active ingredients from MCs is crucial for enhancing efficacy and extending the functional lifespan of pesticides. This study investigated the release profiles of Pyr from various PU MCs to validate their sustained release characteristics. The cumulative release curves for Pyr@PU MCs and Pyr@KCeO2-PU MCs are presented in Fig. 3A. Initially, a rapid release of Pyr was observed from the different PU MCs, followed by a gradual decrease in the release rate. This phenomenon can be attributed to the Pyr molecules located on the surface layer of the PU MCs, which are readily released into the surrounding medium, whereas the internal Pyr molecules must diffuse to the outer layer before they can be released [39]. This sustained release of Pyr facilitates the maintenance of an effective long-term concentration, thereby prolonging insecticidal activity. Notably, the release rate and cumulative release of Pyr@KCeO2-PU MCs were superior to those of Pyr@PU MCs. Within the first 24 h, Pyr@KCeO2-PU MCs exhibited a more rapid release, with cumulative release amounts of

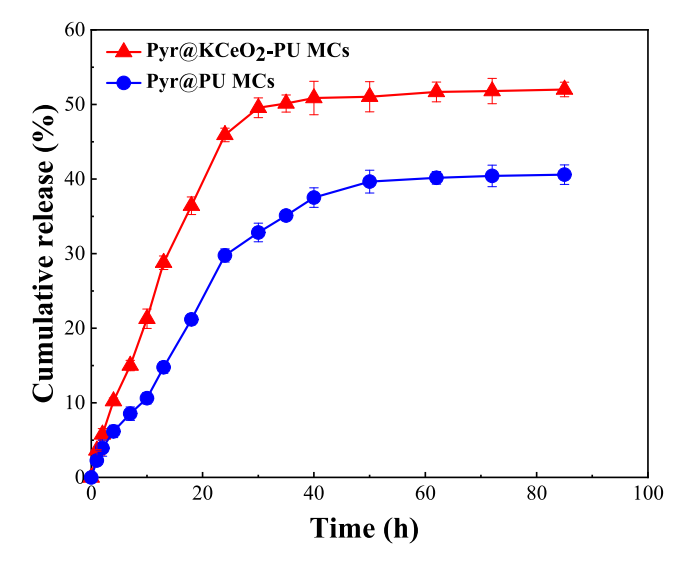


Fig. 3. Cumulative release curve of Pyr@PU MCs and Pyr@KCeO2-PU MCs.

approximately 46 % for Pyr@KCeO $_2$ -PU MCs compared to 29 % for Pyr@PU MCs. Furthermore, after 50 h, both formulations reached a state of release equilibrium, with cumulative release percentages of 53 % for Pyr@KCeO $_2$ -PU MCs and 40 % for Pyr@PU MCs. This study demonstrates that the incorporation of CeO $_2$ into the PU shell can effectively modulate the drug release rate.

To investigate the release mechanism of Pyr from MCs, we analyzed the release profile utilizing the empirical equations (Zero-order, First-order, Higuchi, and Ritger-Peppas mathematical models) presented in Table 1 and depicted in Fig. S3. Both Pyr@PU MCs and Pyr@KCeO $_2$ -PU MCs demonstrated release patterns that are more consistent with the first-order kinetic model, exhibiting high fitting coefficients (R $^2 > 0.98$). indicating that the release behavior belong to non-Fickian behavior controlled by dissolution and diffusion. This suggests that the drug release kinetics of the MCs involved an initial rapid release phase, followed by a sustained release occurring after 30 h.

Table 1 Cumulative release curve kinetic fitting of Pyr@PU MCs and Pyr@KCeO $_2$ -PU MCs.

Model	Equation	R ²	
		Pyr@KCeO ₂ -PU MCs	Pyr@PU MCs
Zero-order	Q = a + bt	0.6796	0.8005
First-order	$Q = a(1-e^{-bt})$	0.9860	0.9827
Higuchi	$Q = a + bt^{1/2}$	0.6796	0.8005
Korsmeyer-Peppas	$Q = bt^n$	0.8912	0.9250

3.5. Photostability of Pyr-loaded MCs

The photodegradation of pesticides following application severely undermines their efficacy and significantly affects their longevity and utilization efficiency. Encapsulation technology serves as a crucial method for enhancing the optical stability of pesticides by embedding them within capsule shells, thereby preventing photodegradation and reducing the release rate of the pesticide [40]. As illustrated in Fig. 4A, the decomposition rate of the encapsulated Pyr was markedly lower compared to that of Pyr TC. Noteworthy differences in the retention percentage of Pyr were recorded across various samples after 100 h of UV exposure. Pyr TC demonstrated rapid degradation under UV radiation, with only 20 % remaining after this duration. In contrast, Pyr encapsulated in Pyr@PU MCs and Pyr@KCeO2-PU MCs exhibited significantly enhanced stability, with cumulative residual rates of 30 %and 38 %, respectively, after 100 h of irradiation. It is evident that Pyr@KCeO₂-PU MCs provide superior UV protection, approximately 1.9 times greater than that of Pyr TC. These findings indicate that the modification of Pyr@PU MCs with CeO2 substantially enhances the stability of Pyr against UV degradation, attributed to the exceptional UV absorption properties of CeO₂, which effectively mitigate pesticide deactivation.

The UV degradation curve was analyzed utilizing pseudo-first-order kinetics [41] to determine the degradation half-life, calculated using the formula $t_{1/2}=\ln 2/k$. The results are illustrated in Fig. 4B and summarized in Table 2. Pyr@KCeO_2-PU MCs exhibited superior photostability, with a half-life ($t_{1/2}$) of 55.63 h under UV light, outperforming Pyr@PU MCs ($t_{1/2}=43.19$ h) and Pyr TC ($t_{1/2}=29.53$ h). This indicates that Pyr@KCeO_2-PU MCs and Pyr@PU MCs demonstrate photostability levels approximately 1.9 and 1.5 times greater than that of Pyr TC, respectively. These findings imply that encapsulating Pyr within PU MCs serves as an effective physical barrier against UV light. Importantly, the exceptional UV-filtering properties of CeO_2 nanoparticles in Pyr@K-CeO_2-PU MCs significantly enhance the anti-UV performance, thereby improving the photostability of Pyr. The proposed mechanism for the

Table 2Fitting results for the data of photodegradation of different samples.

Equation	Simple	k(h ⁻¹)	t _{1/2} (h)
$y = exp^{-kt}$	Pyr TC	0.02347	29.53
	Pyr@PU MCs	0.01605	43.19
	Pyr@KCeO ₂ -PU MCs	0.01246	55.63

UV resistance of Pyr@KCeO $_2$ -PU MCs is depicted in Fig. 4D, which involves (i) reduced UV transmittance through the PU shell [42] and (ii) UV light absorption by CeO $_2$ nanoparticles [43]. Given their robust photostability and adhesion characteristics (as shown in Fig. 7), Pyr@KCeO $_2$ -PU MCs can effectively adhere to plant leaves upon application, thereby providing long-term protection for crop growth and minimizing the necessity for frequent pesticide applications and dosages.

The ultraviolet radiation that reaches the Earth primarily consists of UV-A and UV-B, with wavelengths ranging from 280 to 400 nm. Ultraviolet light possesses shorter wavelengths and higher radiant energy compared to visible light. Pyr TC is particularly unstable when exposed to ultraviolet radiation, rendering it vulnerable to damage. To mitigate the decomposition of Pyr within microcapsules due to UV exposure, it is essential to enhance the absorbance of the polymer carrier within this wavelength range. Fig. 4C illustrates the UV-Vis spectra of Pyr TC, Pyr@PU MCs, and Pyr@KCeO2-PU MCs across the 200-380 nm spectrum. The absorption peak associated with Pyr is not distinctly observable in Pyr@PU MCs and Pyr@KCeO₂-PU MCs, owing to overlapping absorption bands. Notably, the absorption values for Pyr@PU MCs and Pyr@KCeO₂-PU MCs in the 200-380 nm range are significantly elevated compared to those of Pyr TC, which can be attributed to the absorption characteristics of urea and urethane bonds present in the polymeric shell of the MCs. Specifically, Pyr@KCeO2-PU MCs, which are modified with CeO2 NPs, demonstrate enhanced UV absorption, indicating improved UV protection for Pyr. These results suggest that Pyr@KCeO2-PU MCs exhibit superior efficacy in shielding against photodegradation, thereby

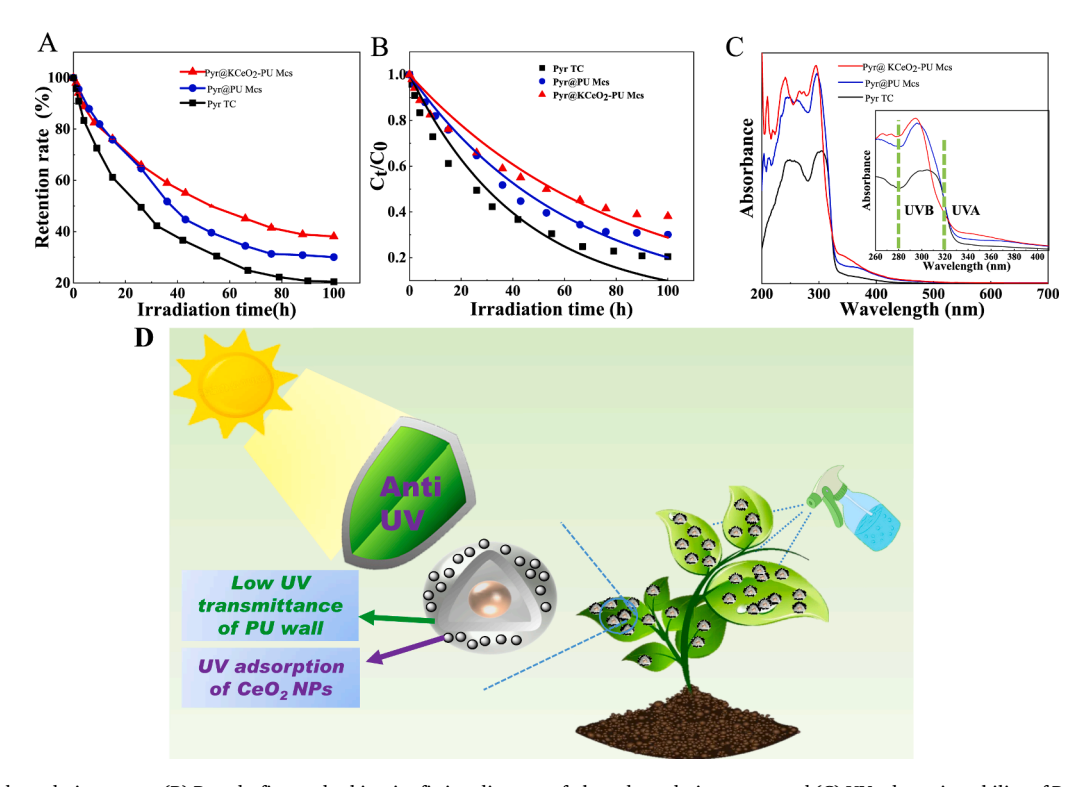


Fig. 4. (A) Photodegradation curve, (B) Pseudo-first-order kinetics fitting diagram of photodegradation curve and (C) UV adsorption ability of Pyr TC. Pyr@PU MCs and Pyr@KCeO₂-PU MCs. (D) Potential mechanism of UV resistance of Pyr@KCeO₂-PU MCs.

extending the effectiveness of Pvr.

3.6. Rheological properties of PU MCs

The significance of apparent viscosity and thixotropy in evaluating the stability of suspension concentrate is emphasized in previous research [13]. An investigation into the rheological properties of Pyr@KCeO₂-PU MCs demonstrated a pronounced shear-thinning behavior that occurs with increasing shear rates, as illustrated in Fig. 5. This behavior indicates that the sample behaves as a non-Newtonian fluid, which facilitates its spread out on leaf surfaces [44]. The shear-thinning phenomenon can be attributed to the preferential alignment of networks structures along the flow direction, thereby reducing local viscous drag. At elevated shear rates, network segments align more completely with the flow field, resulting in a reduction of shear viscosity [45,46]. This shear-thinning characteristic is particularly advantageous for the application of Pyr@KCeO2-PU MCs in spraying, as it enables a lower viscosity during mixing, which assists in the uniform distribution of active ingredients. Additionally, maintaining a low viscosity during storage is crucial for ensuring optimal stability against settling or sedimentation due to gravity [47,48]. Overall, the shearthinning property enhances both the flowability and stability of the dispersion. At a shear rate of 100 s⁻¹, the viscosity reaches a constant minimum value, indicating the complete disruption of the threedimensional network structure. This variation in apparent viscosity with shear rate is beneficial for the encapsulation and controlled release of pesticides within Pyr@KCeO2-PU MCs [49].

The "three-stage" thixotropic test is typically employed to investigate the viscosity recovery of suspension systems, thereby elucidating the potential relationship between viscosity and changes in network structure [17]. The recovery of apparent viscosity serves as an indicator of the ability of suspension systems to re-establish their internal microstructure, which is crucial for preventing the separation of solid-liquid phases and maintaining suspension stability [50]. As illustrated in Fig. 5C, the sample exhibited a relatively high apparent viscosity at a shear rate of 0.25 s⁻¹, which sharply decreased as the shear rate increased to 1000 s⁻¹. Upon returning to a low shear rate of 0.25 s⁻¹, the apparent viscosity rapidly recovered, achieving a recovery rate of approximately 94 %. According to previous studies, a recovery rate exceeding 70 % is considered indicative of good thixotropic recovery [51], which suggests the reconstruction of the structural network and is beneficial for the long-term storage of suspensions. Furthermore, pesticides can withstand high shear pressure and form droplets when sprayed through a nozzle [52]. The viscosity of the spray mixture significantly influences the size of the droplets produced by the atomizer. The shear-thinning property of the sample facilitates easy atomization [53], thereby enhancing the physical stability of Pyr@KCeO2-PU MCs, which is advantageous for high-speed spraying.

3.7. Wettability and adhesion ability

The superhydrophobic characteristics of crop leaves impede the spreading and wetting of droplets, thereby presenting a significant challenge to the effective deposition and long-term adhesion of pesticides. The wettability and adhesion of pesticide droplets on crop leaves are essential for enhancing pesticide deposition rates and utilization [54]. Notably, smaller contact angles are typically more effective in preventing droplets from rolling off leaf surfaces [55,56]. The wettability of Pyr@KCeO2-PU MCs and Pyr@PU MCs was assessed by measuring the dynamic contact angles on rice leaves (Fig. 6A, C). A smaller contact angle is advantageous in preventing droplets from sliding off the plant leaves. The contact angle of water on the rice leaf was measured at 114°, showing minimal changes, which indicates that the rice leaf is hydrophobic. The contact angles of Pyr@PU MCs decreased from 100° to 84° over 300 s, whereas the contact angle of Pyr@KCeO2-PU MCs decreased from 43.05° to 32° in comparison to water. The incorporation of KCeO2 significantly reduces the contact angle of Pyr@KCeO2-PU MCs, leading to enhanced adhesion to rice leaves. This enhancement is attributed to the addition of hydrophobic KH-550, a compound frequently employed to strengthen interactions between particles and superhydrophobic surfaces [57]. Furthermore, KH-550 plays a vital role in facilitating crosslinking between PU and CeO₂ [58].

Liquid holding capacity (LHC) on the leaves is a critical factor in evaluating the wettability of pesticides, which subsequently influences the deposition of active ingredients on foliage [59]. Enhanced foliar retention contributes to resistance against rain erosion, improves the retention of the pesticide on leaves, and increases the protective effects of the treatment [60]. To investigate the foliar retention of the samples on rice leaves, the LHC of the formulation was measured on rice leaves (Fig. 6B). The results indicated that the retention of Pyr from Pyr@K-CeO₂-PU MCs on rice leaves was 17.5 mg/cm², significantly surpassing that of Pyr@PU MCs, which was only 9.3 mg/cm². This finding suggests that Pyr@KCeO₂-PU MCs possess superior leaf adhesion properties, resulting in greater retention of Pyr following flushing. Consequently, the residual rate of Pyr@KCeO₂-PU MCs after flushing was approximately 58 %, more than double the residual rate of Pyr@PU MCs, which was 26 %.

To visualize the foliar retention performance, fluorescence microscopy was employed to assess the retention and flush resistance of Pyr@KCeO₂-PU MCs. The initial image captured before flushing served as a baseline for 100 % coverage, followed by an evaluation of the attachment of Pyr@KCeO₂-PU MCs after flushing. Prior to flushing, the leaf surface exhibited complete coverage with green fluorescence, as illustrated in Fig. 6D. Notably, Pyr@KCeO₂-PU MCs with green fluorescence remained clearly visible on the surface of rice leaves after being sprayed and subsequently flushed with water at a 60° angle. This observation demonstrates that Pyr@KCeO₂-PU MCs possess significant

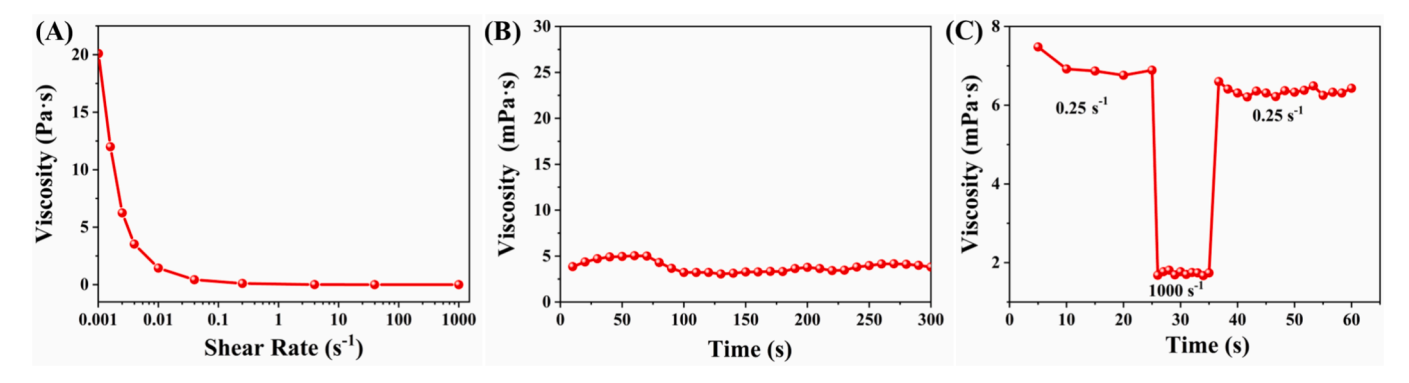


Fig. 5. (A) Shear viscosity versus shear rate of Pyr@KCeO₂-PU MCs; (B) Viscosity of Pyr@KCeO₂-PU MCs under the fixed shear rate of 10.48 s^{-1} ; (C) Hixotropism of the Pyr@KCeO₂-PU MCs: the shear rate was 0.25 (s^{-1}) from 0 to 25 (s), 1000 (s^{-1}) from 25 to 35 (s), and 0.25 (s^{-1}) from 35 to 60 (s).

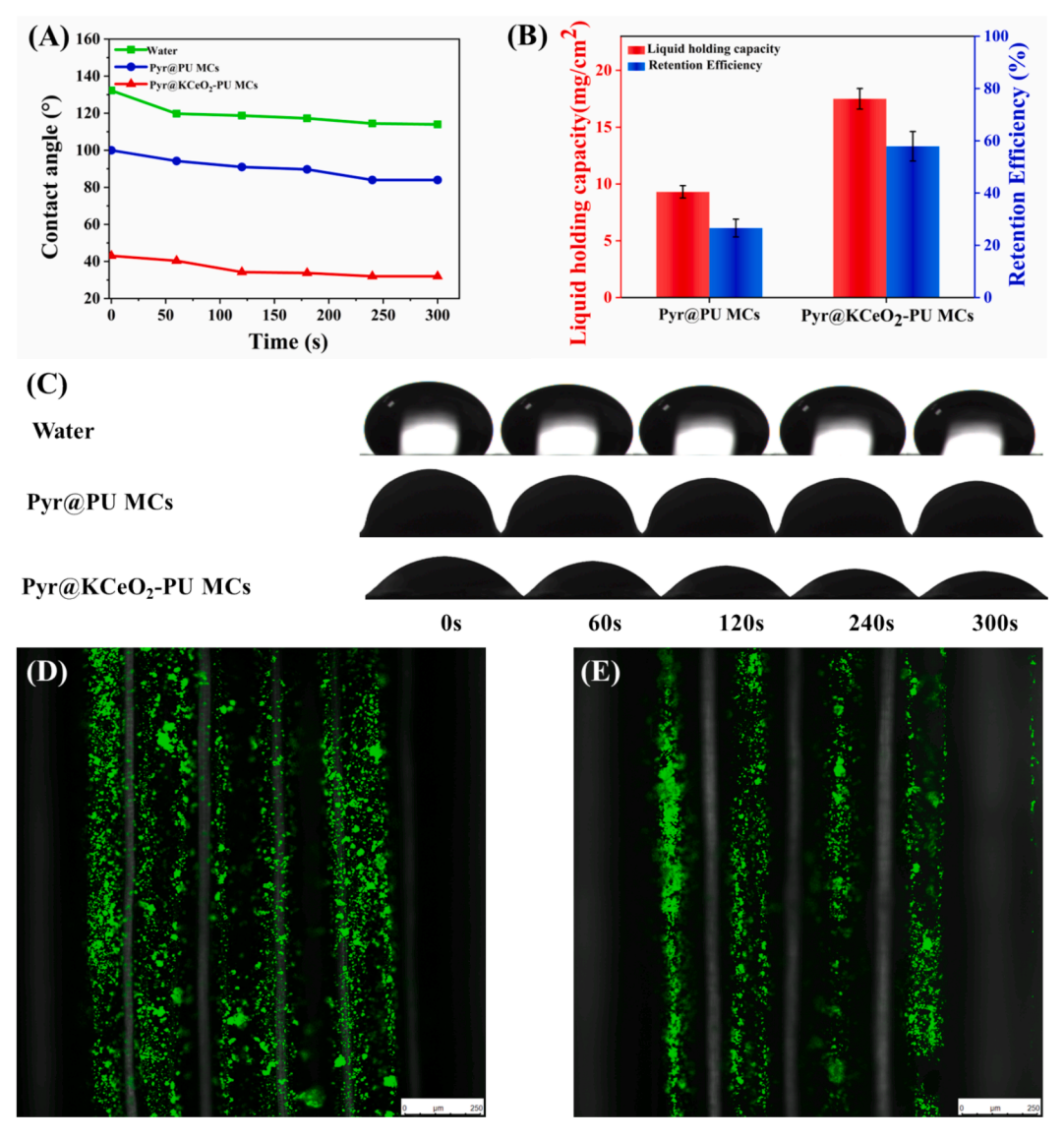


Fig. 6. (A, C) The contact angles of Pyr@KCeO₂-PU MCs and Pyr@PU MCs on leaves and their changes up to 300 s; (B) Liquid holding capacities of Pyr@KCeO₂-PU MCs and Pyr@PU MCs, and retention efficiency after the simulated rain erosion experiment. Pyr@KCeO₂-PU MCs simulated fluorescence microscopy (D) before and (E) after rain wash.

resistance to rainwater erosion and exhibit superior adhesion, effectively preventing the wash-off of pesticides by rainwater. Overall, Pyr@KCeO₂-PU MCs were shown to enhance the deposition and spreading of active ingredients on rice leaves. When sprayed onto the plant foliage, the active ingredients that adhered to the leaves and resisted rain erosion contributed to an increased utilization rate of these active ingredients.

3.8. Cytotoxicity

Considering the toxicity of pesticides, it is crucial to explore the hazards that pesticides pose to humans when used [61]. Human LO2 cells were used to explore the cytotoxicity of Pyr@KCeO2-PU MCs by means of cell proliferation and apoptosis, and further simulated to assess their effects on humans. Fig. 7 shows that the survival rate of LO2 cells was significantly higher for Pyr@KCeO2-PU MCs than for Pyr TC. Meanwhile, the toxicity of Pyr@KCeO2-PU MCs was also lower than the commercial preparation Seltima to LO2 cells. The above results indicated that Pyr@KCeO2-PU MCs had a weaker effect on the human body. Given the toxicity of pesticides, it is essential to investigate the

hazards they pose to human health [61]. In this study, human LO2 cells were utilized to assess the cytotoxicity of Pyr@KCeO2-PU MCs through cell proliferation and apoptosis assays, with further simulations conducted to evaluate their effects on humans. Fig. 7 illustrates that the survival rate of LO2 cells exposed to Pyr@KCeO2-PU MCs was significantly higher compared to those treated with Pyr TC. Additionally, the toxicity of Pyr@KCeO2-PU MCs was found to be lower than that of the commercial preparation Seltima when applied to LO2 cells. These results suggest that Pyr@KCeO2-PU MCs exert a milder impact on human health.

3.9. Antifungal activity evaluation.

The effects of Pyr@KCeO₂-PU MCs, Pyr TC, and Seltima on various fungal pathogens, including *rice blast fungus, cucumber cinerea, rice sheath blight, anthracnose, soot, and Sclerotinia sclerotiorum*, were evaluated using the mycelial growth rate method to assess inhibitory activity (Fig. 8). Concurrently, the biological activity of blank PU MCs was also assessed. The data presented in the figure indicate that at an active ingredient concentration of $1 \mu g/mL$, $Pyr@KCeO_2-PU$ MCs, Pyr TC, and

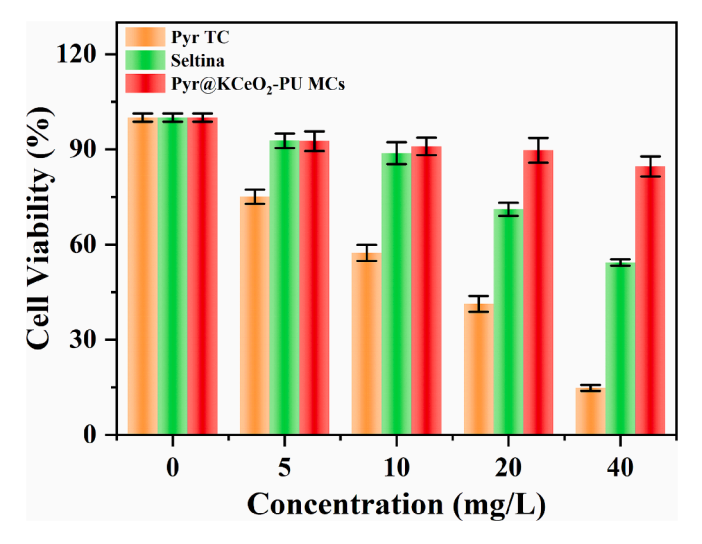


Fig. 7. The cell viability of LO2 cells after incubated with Pyr TC, Seltima and $Pyr@KCeO_2$ -PU MCs for 24 h.

Seltima exhibited significant biological activity against all six fungal strains. Notably, the strongest inhibitory effect was observed against rice sheath blight, with inhibition rates ranging from 73.48 \pm 2.43 % to 83.30 \pm 3.85 %. Conversely, the inhibitory activity against Sclerotinia sclerotiorum was comparatively weaker, with rates between 37.96 \pm 2.09 % and 40.90 \pm 3.97 %. These findings suggest that the inhibitory effects of Pyr@KCeO2-PU MCs, Pyr TC, and Seltima on the tested fungal strains are comparable.

4. Conclusion

In this study, we successfully developed a highly effective polyurethane-inorganic hybrid microcapsule system (Pyr@KCeO2-PU MCs) that exhibits excellent anti-UV properties and wettability. This system was created through interfacial polymerization using Pyr as a model photosensitive pesticide and CeO₂ as a UV light absorber. The robust UV-shielding properties of the PU shell, combined with the UVabsorption capabilities of CeO2, enable Pyr@KCeO2-PU MCs to effectively protect Pyr from photodegradation, thereby enhancing its photostability. In comparison to Pyr@PU MCs, the incorporation of GeO2 modified by KH550 significantly reduces the contact angle of Pyr@K-CeO₂-PU MCs, leading to improved foliar adhesion and wettability. Furthermore, Pyr@KCeO2-PU MCs exhibited superior efficacy in controlling various pathogens, achieving control levels comparable to those of Pyr TC and Seltima. In summary, this research presents a promising strategy for protecting UV-sensitive pesticides, thereby enhancing their effectiveness in disease management and improving safety profiles. The Pyr@KCeO2-PU MCs formulation significantly enhances the field application of Pyr, thereby broadening its potential uses in the management of rice diseases and improving its commercial viability. This development holds considerable practical significance.

CRediT authorship contribution statement

Nianlei Zhang: Writing – original draft. Yanan Xiao: Methodology. Shuhui Hu: Investigation. Qian Chen: Formal analysis. Yan Huang: Conceptualization. Mengdie Li: Software. Zijing Jin: Formal analysis. Huaixiang Chen: Formal analysis. Wenneng Wu: Funding acquisition. Jian Wang: Visualization, Validation. Bo Zhang: Writing – original draft.

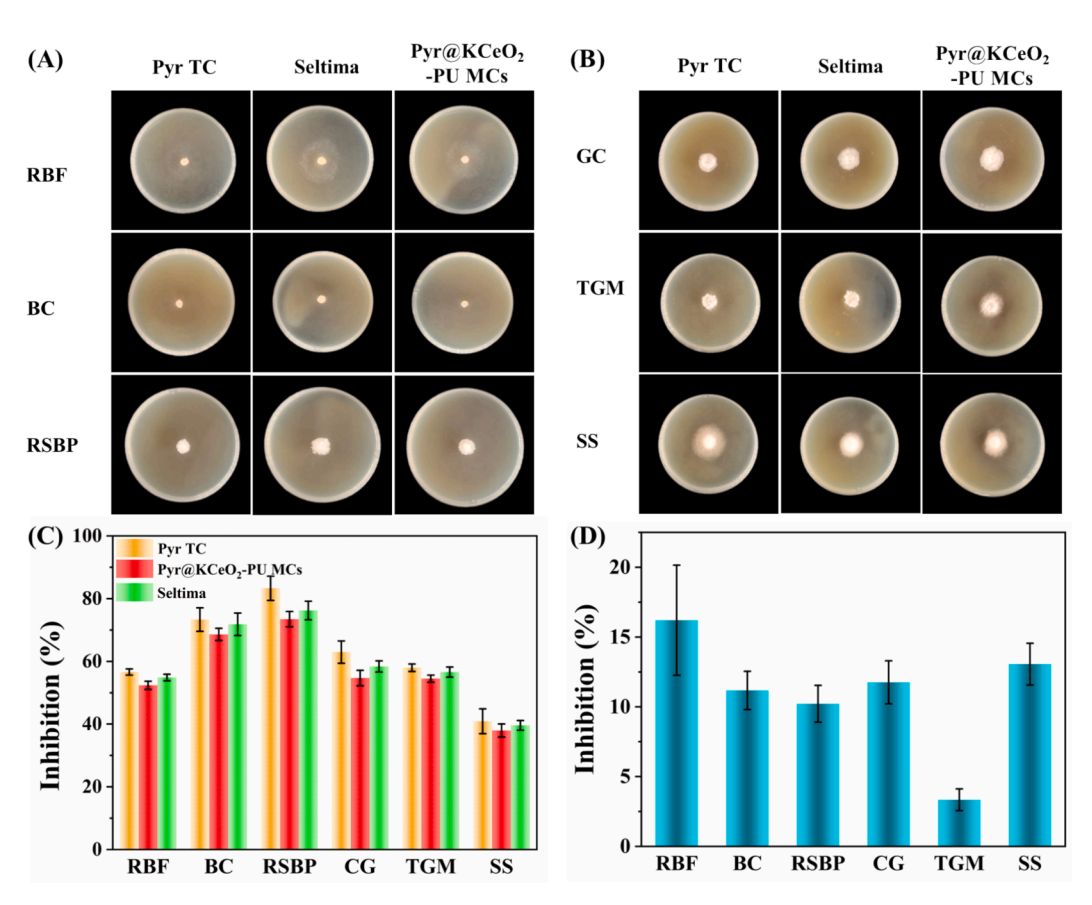


Fig. 8. (A and C) Inhibitory activities of Pyr TC, Seltima and Pyr@KCeO₂-PU MCs against different fungi at the concentration of 1 μ g/mL; (B and D) Inhibitory activity of Blank PU MCs against different fungi at a concentration of 100 μ g/mL (RBF = rice blast, BC = cinerea cinerea, RSBP = rice sheath blight, CG = anthracnose, TGM = soot enzyme, SS = rapeseed sclerotia).

Declaration of competing interest

The authors declare that they have no known competing financial interests or personal relationships that could have appeared to influence the work reported in this paper.

Acknowledgments

This work was sponsored by Shanghai Sailing Program (22YF1431300); The Science and Technology Fund Project of Guizhou (No. Qian Ke He Pingtai Rencai-CXTD [2022] 002); The Science and Technology Planning Project of Guizhou Province (No. QKHZC [2022] 132). We appreciate eceshi (www.eceshi.com) for the TGA test.

Appendix A. Supplementary data

Supplementary data to this article can be found online at https://doi.org/10.1016/j.cej.2024.157351.

Data availability

Data will be made available on request.

References

- M. Nehra, N. Dilbaghi, G. Marrazza, A. Kaushik, C. Sonne, K.H. Kim, S. Kumar, Emerging nanobiotechnology in agriculture for the management of pesticide residues, J. Hazard. Mater. 401 (2021) 123369, https://doi.org/10.1016/j. ihazmat.2020.123369.
- [2] H.Y. Chen, J.H. Zhan, L. Man, H.K. Deng, H.J. Zhou, L. Hao, X.H. Zhou, High foliar retention tannic acid/Fe³⁺ functionalized Ti-pillared montmorillonite pesticide formulation with pH-responsibility and high UV stability, Appl. Surf. Sci. 620 (2023) 156838, https://doi.org/10.1016/j.apsusc.2023.156838.
- [3] H. Chen, H. Zhi, B. Feng, B. Cui, X. Zhao, C. Sun, Y. Wang, H. Cui, B. Zhang, Z. Zeng, Thermo-responsive quaternary ammonium chitosan nanocapsules with ondemand controlled pesticide release and maximally synergistic biological activity, J. Agric. Food Chem. 70 (2022) 7653–7661, https://doi.org/10.1021/acs. iafc 2c01701
- [4] P.T. Deota, H.S. Parmar, G.M. Patel, G.J. Bhatt, Impact of ultraviolet-absorbing 2-hydroxy-4-quaternaryammoniumalkoxy benzophenone motif on photodegradation of disulfoton: a case study, Environ. Sci. Pollut. Res. 29 (2022) 89108–89120, https://doi.org/10.1007/s11356-022-21247-1.
- [5] Z. Wei, J.X. Zhu, Y. He, J. Lai, B.J. Pan, K.Y. Feng, L.H. Chen, L.D. Cao, Y. Wang, K. Qian, Improving the efficiency and environmental safety of emamectin benzoate through a pH-responsive metal-organic framework microencapsulation strategy, J. Hazard. Mater. 475 (2024) 134847, https://doi.org/10.1016/j.jhazmat.2024.134847.
- [6] Z.Y. Zhou, G. Tang, Y.L. Liu, X.H Zhang, Y.Q. Huang, J.L. Wang, G.Y. Yan, G.H. Hu, J.H Xiao, W.Y. Yan, Y.S. Cao, Facile fabrication of pesticide nanocapsules using cinnamaldehyde derived imide polymer as wall material for pH-responsive and ultraviolet shielding properties, Chem. Eng. J. 489 (2024) 151430, https://doi.org/10.1016/j.cej.2024.151430.
- [7] R. Wang, S. Liu, F.S. Sun, X. Yu, X. Liu, B.X. Li, W. Mu, D.X. Zhang, F. Liu, Balance the rapid release of insecticide microcapsules using double-layer shielding effect when the foliar application, Chem. Eng. J. 455 (2023) 140899, https://doi.org/ 10.1016/j.cej.2022.140899.
- [8] L. Chen, W. Zhang, H. Du, X. Ding, L. Li, H. Chen, F. Gao, B. Cui, J. Gao, H. Cui, Y. Yao, Z. Zeng, Enhancing safety through the biodegradable pesticide microcapsules produced via melt emulsification and interfacial polymerization, Chem. Eng. J. 483 (2024) 149407, https://doi.org/10.1016/j.cej.2024.149407.
- [9] G. Chen, W.J. Shangguan, H.P. Chen, C.L. Xu, M. Bilal, P.Y. Zhao, C. Cao, M.L. Yu, Q.L. Huang, L.D. Cao, Chitooligosaccharide modified pesticide-loaded polyurethane microcapsules to mitigate drought stress in wheat, Chem. Eng. J. 479 (2024) 147688, https://doi.org/10.1016/j.cej.2023.147688.
- [10] Y. Chen, Z. Li, C. Han, H. Cao, X. Jian, H. Sun, H. Xiao, P. Zhang, X. Zhao, N. Zou, F. Liu, H. Dong, D. Zhang, Lignin microcapsules prepared on the basis of flexible skeleton with high foliar retention and UV shielding properties, Int. J. Biol. Macromol. 273 (2024) 132944, https://doi.org/10.1016/j.ijbiomac.2024.132944.
- [11] H. Chen, H. Zhi, J. Liang, M. Yu, B. Cui, X. Zhao, C. Sun, Y. Wang, H. Cui, Z. Zeng, Development of leaf-adhesive pesticide nanocapsules with pH-responsive release to enhance retention time on crop leaves and improve utilization efficiency, J. Mater. Chem. B 9 (2021) 783–792, https://doi.org/10.1039/d0tb02430a.
- [12] H. Cao, Y. Chen, Z. Qian, T. Huang, N. Zou, D. Zhang, W. Mu, B. Li, F. Liu, Amphiphilicity-driven small alcohols regulate the flexibility of pesticide-loaded microcapsules for better foliar adhesion and utilization, ACS Appl. Mater. Interfaces 15 (2023) 21444–21456, https://doi.org/10.1021/acsami.3c01221.
- [13] J. Wang, Z. Shi, G. Yuan, N. Zhang, Y. Xiao, Z. Jin, M. Li, W. Wu, Y. Yuan, T. Ren, B. Zhang, A flexible modulated pesticide release platform through poly

- (urethane-urea) microcapsules: effect of different crosslinkers compositions, Pest Manag. Sci. 80 (2024) 3707–3716, https://doi.org/10.1002/ps.8073.
- [14] T. Zhang, H. Sun, L. Yang, P. Zhang, Y. Zhang, J. Bai, F. Liu, D. Zhang, Interfacial polymerization depth mediated by the shuttle effect regulating the application performance of pesticide-loaded microcapsules, ACS Nano 17 (2023) 20654–20665, https://doi.org/10.1021/acsnano.3c07915.
- [15] H. Cao, D.X. Zhang, S. Liu, J. Luo, T. Jing, S. Pan, F. Liu, B. Li, W. Mu, Achieving win-win ecotoxicological safety and fungicidal activity of pyraclostrobin-loaded polyurea microcapsules by selecting proper polyamines, J. Agr. Food Chem. 69 (2021) 2099–2107, https://doi.org/10.1021/acs.jafc.0c07482.
- [16] J. Wang, R. Wang, Z.F. Shi, R.T. Zeng, R. Ren, B. Zhang, Glutathione-responsive pyraclostrobin-loaded polyurea microcapsules for their intelligent controlled release, J. Agric. Food. Chem. 70 (2022) 5310–5318, https://doi.org/10.1021/acs. iafc.1c08182.
- [17] B.B. Jiang, R.H. Li, X. He, Y.L. Chai, Y.X. Chai, Y. Wang, Fabrication PDA-polyurea microcapsules with anti-photolysis and sustained-release performances via Pickering emulsion template, Colloid. Polym. Sci. 300 (2021) 1–10, https://doi. org/10.1007/s00396-021-04922-6.
- [18] T. Zheng, K. Chen, W.Y. Chen, B. Wu, Y. Sheng, Y. Xiao, Preparation and characterisation of polylactic acid modified polyurethane microcapsules for controlled-release of chlorpyrifos, J. Microencapsul. 36 (2019) 62–71, https://doi. org/10.1080/02652048.2019.1599075.
- [19] H.C. Cao, Y. Chen, D.X. Zhang, Y. Jin, P. Zhang, B.X. Li, W. Mu, F. Liu, Octaphenyl polyoxyethylene regulates the flexibility of pyraclostrobin-loaded soft microcapsules by interfacial polymerization for better foliar adhesion and pesticide utilization, Chem. Eng. J. 439 (2022) 135805, https://doi.org/10.1016/j.cei.2022.135805.
- [20] Y.X. Pang, X. Li, S.W. Wang, X.Q. Qiu, D.J. Yang, H.M. Lou, Lignin-polyurea microcapsules with anti-photolysis and sustained-release performances synthesized via pickering emulsion template, React. Funct. Polym. 123 (2018) 115–121, https://doi.org/10.1016/j.reactfunctpolym.2017.12.018.
- [21] R.A. Feldbaum, N. Yaakov, K.A. Mani, E. Yossef, S. Metbeev, E. Zelinger, E. Belausov, H. Koltai, D. Ment, G. Mechrez, Single cell encapsulation in a Pickering emulsion stabilized by TiO₂ nanoparticles provides protection against UV radiation for a biopesticide, Colloid Surface B 206 (2021) 111958, https://doi.org/ 10.1016/j.colsurfb.2021.111958.
- [22] N.M. Zholobak, V.K. Ivanov, A.B. Shcherbakov, A.S. Shaporev, O.S. Polezhaeva, A. Y. Baranchikov, N.Y. Spivak, Y.D. Tretyakov, UV-shielding property, photocatalytic activity and photocytotoxicity of ceria colloid solutions, J. Photoch. Photobio. B 102 (2011) 32–38. https://doi.org/10.1016/j.jphotobiol.2010.09.002.
- [23] B. Wang, F. Jiang, X. Ma, Z. Dong, Y. Liu, Preparation of highly dispersed ZnO nanoparticles to fabricate ultraviolet-shielding poly(vinyl chloride) films, Colloid Polym. Sci. 300 (2021) 51–57, https://doi.org/10.1007/s00396-021-04929-z.
- [24] H.K. Singh, S. Kumar, J. Bamne, K. Taiwade, N. Singh, V. Chandel, F.Z. Haque, Analyzing the synthesis of various inorganic nanoparticles and their role in UVshielding, Mater. Today 46 (2021) 5607–5618, https://doi.org/10.1016/j. matpr.2020.09.499.
- [25] R. Huang, X. Du, H. Wang, X. Cheng, Z. Du, Highly stretchable polyurethane coating based on functionalized cerium oxide nanoparticles for anti-corrosive/UV protection, J. Appl. Polym. Sci. 139 (2022) 51927, https://doi.org/10.1002/ ann 51927
- [26] M.M. Rahman, R. Suleiman, M.H. Zahir, A. Helal, A.M. Kumar, M.B. Haq, Multi Self-healable UV shielding polyurethane/CeO₂ protective coating: the effect of low-molecular-weight polyols, Polymers 12 (2020) 1947, https://doi.org/10.3390/polym12091947.
- [27] A. Saadat-Monfared, M. Mohseni, Polyurethane nanocomposite films containing nano-cerium oxide as UV absorber; Part 2: Structural and mechanical studies upon UV exposure, Colloid Surface A 441 (2014) 752–757, https://doi.org/10.1016/j. colsurfa.2012.10.064.
- [28] Y. Ma, M. Yu, Y. Wang, S. Pan, X. Sun, R. Zhao, Z. Sun, R. Gao, X. Guo, Y. Xu, X. Wu, A pH/cellulase dual stimuli-responsive cellulose-coated metal-organic framework for eco-friendly fungicide delivery, Chem. Eng. J. 462 (2023) 142190, https://doi.org/10.1016/j.cej.2023.142190.
- [29] X. Zhang, J. Niu, Z. Zhou, G. Tang, G. Yan, Y. Liu, J. Wang, G. Hu, J. Xiao, W. Yan, Y. Cao, Stimuli-responsive polymeric micelles based on cellulose derivative containing imine groups with improved bioavailability and reduced aquatic toxicity of pyraclostrobin, Chem. Eng. J. 474 (2023) 145789, https://doi.org/10.1016/j.cej.2023.145789.
- [30] M. Li, Z.X. Shi, Z.G. Liu, Y.H. Hu, M.T. Wang, H.Q. Li, Effect of surface modification on behaviors of cerium oxide nanopowders, J. Rare Earth 25 (2007) 368–372, https://doi.org/10.1016/S1002-0721(07)60438-4.
- [31] L.R. Zeng, L.H. Shi, X.G. Meng, J. Xu, G.F. Jia, T. Gui, D.Y. Hu, Evaluation of photolysis and hydrolysis of pyraclostrobin in aqueous solutions and its degradation products in paddy water, J. Environ. Sci. Health B 54 (2019) 317–325, https://doi.org/10.1080/03601234.2019.1571360.
- [32] H.S. Nanda, Surface modification of promising cerium oxide nanoparticles for nanomedicine applications, RSC Adv. 6 (2016) 111889–111894, https://doi.org/ 10.1039/C6RA23046F.
- [33] A.H. Zou, Y. Yang, J.G. Cheng, V.M. Garamus, N. Li, Construction and characterization of a novel sustained-release delivery system for hydrophobic pesticides using biodegradable polydopamine-based microcapsules, J. Agric. Food Chem. 66 (2018) 6262–6268, https://doi.org/10.1021/acs.jafc.8b00877.
- [34] D.X. Xiao, W.L. Liang, Z.G. Xie, J.L. Cheng, Y.J. Du, J.H. Zhao, A temperature-responsive release cellulose-based microcapsule loaded with chlorpyrifos for sustainable pest control, J. Hazard Mater. 403 (2021) 123654, https://doi.org/10.1016/j.jhazmat.2020.123654.

- [35] R.Y. Dai, S.Y. You, L.M. Lu, Q. Liu, Z.X. Li, L. Wei, X.G. Huang, Z.Y. Yang, High blades spread ability of chlorpyrifos microcapsules prepared with polysiloxane sodium carboxylate/sodium carboxymethylcellulose/gelatin via complex coacervation, Colloid Surface A 530 (2017) 13–19, https://doi.org/10.1016/j. colsurfa.2017.06.057.
- [36] P.F. Shan, Y.W. Lu, W.L. Lu, X.P. Yin, H.W. Liu, D.A. Li, X.Y. Lian, W.P. Wang, Z. Y. Li, Z.H. Li, Biodegradable and light-responsive polymeric nanoparticles for environmentally safe herbicide delivery, ACS Appl. Mater. Interfaces 14 (2022) 43759–43770, https://doi.org/10.1021/acsami.2c12106.
- [37] M. Pourmohammadi-Mahunaki, V. Haddadi-Asl, H. Roghani-Mamaqani, M. Koosha, M. Yazdi, Effect of chain extender length and molecular architecture on phase separation and rheological properties of ether-based polyurethanes, Polym. Bull 79 (2021) 8653–8668, https://doi.org/10.1007/s00289-021-03907-3.
- [38] J. Feng, Z. Chen, W. Chen, L. Sun, J. Yang, K. He, S. Dong, S. Yuan, Facile pathway to construct mesoporous silica nanoparticles loaded with pyraclostrobin: physicochemical properties, antifungal activity, and biosafety, Pest Manag. Sci. 78 (2022) 2332–2341, https://doi.org/10.1002/ps.6859.
- [39] J. Luo, D.X. Zhang, T.F. Jing, G. Liu, H.C. Cao, B.X. Li, Y.M. Hou, F. Liu, Pyraclostrobin loaded lignin-modified nanocapsules: delivery efficiency enhancement in soil improved control efficacy on tomato Fusarium crown and root rot, Chem. Eng. J. 394 (2020) 124854, https://doi.org/10.1016/j. cei.2020.124854.
- [40] Y.J. Ma, L.J. Li, R. Zhao, Z. Sun, Y.M. Wang, M. Yu, S.H. Pan, X. Guo, Y. Xu, H. Wang, P. Wang, X. Wu, Nanoencapsulation-based fabrication of eco-friendly pH-responsive pyraclostrobin formulations with enhanced photostability and adhesion to leaves, J. Environ. Chem. Eng. 11 (2023) 109688, https://doi.org/10.1016/j.jece.2023.109688.
- [41] S.J. Song, M.H. Wan, Y. Luo, H. Shen, J. Shen, Carboxymethyl chitosan-modified graphene oxide as a multifunctional vector for deltamethrin delivery and pHresponsive controlled release, enhanced leaf affinity, and improved mosquitokilling activity, Langmuir 38 (2022) 12148–12156, https://doi.org/10.1021/acs. langmuir.2c01669.
- [42] X. Jia, W. Sheng, W. Li, Y. Tong, Z. Liu, F. Zhou, Adhesive polydopamine coated avermectin microcapsules for prolonging foliar pesticide retention, ACS Appl. Mater Interfaces 6 (2014) 19552–19558, https://doi.org/10.1021/am506458t.
- [43] X.M. Xu, Z.Q. Zhou, L.R. Qin, C.L. Yu, F.A. Zhang, Preparation of PVA/PU/PUA microcapsules and application in self-healing two-component waterborne polyurethane coatings, J. Coat. Technol. Res. 19 (2022) 977–988, https://doi.org/10.1007/s11998-021-00577-8.
- [44] M. Zhao, Z.H. Chen, L. Hao, H.Y. Chen, X.H. Zhou, H.J. Zhou, CMC based microcapsules for smart delivery of pesticides with reduced risks to the environment, Carbohyd. Polym. 300 (2023) 120260, https://doi.org/10.1016/j. carbool.2022.120260.
- [45] S.H. Pan, H.C. Cao, B.X. Li, D.X. Zhang, W. Mu, F. Liu, Improving the efficacy against crop foliage disease by regulating fungicide adhesion on leaves with soft microcapsules, Pest Manag. Sci. 77 (2021) 4418–4424, https://doi.org/10.1002/ ps.6476.
- [46] D.Y. Li, S.Z. Zhang, W.B. Sheng, Q. Zhang, Z.Q. Liu, R. Li, X.H. Liu, C.Y. Meng, C. R. Li, M. Li, X. Jia, Versatile pickering emulsions stabilized by polyphenolic 2D Janus nanosheets enhance foliar deposition of agrochemicals, ACS Appl. Nano Mater. 6 (2023) 8290–8301, https://doi.org/10.1021/acsanm.3c00513.
- [47] K. Hyun, M. Wilhelm, C.O. Klein, K.S. Cho, J.G. Nam, K.H. Ahn, S.J. Lee, R. H. Ewoldt, G.H. McKinley, A review of nonlinear oscillatory shear tests: analysis and application of large amplitude oscillatory shear (LAOS), Prog. Polym. Sci. 36 (2011) 1697–1753, https://doi.org/10.1016/j.progpolymsci.2011.02.002.

- [48] S.P. Zhang, J. Wang, X.D. Yang, B. Zhang, T.R. Ren, Impact of EO chain length of dodecanol ethoxylates (C12En) on the rheological properties and physical stability of pesticide suspension concentrate, Colloid Surface A 627 (2021) 127163, https:// doi.org/10.1016/j.colsurfa.2021.127163.
- [49] S. Kala, A. Agarwal, K. Kant, B.K. Mishra, N. Sogan, N. Kumar, C.K.D. Jawle, D. K. Hazara, J. Kumar, An environmentally benign oil dispersion/phytoextract system for improved retention upon foliage and control of aphids in spice crops, J. Clean Prod. 414 (2023) 137449, https://doi.org/10.1016/j.iclepro.2023.137449.
- [50] S. Saalah, L.C. Abdullah, M.M. Aung, M.Z. Salleh, D.R. Awang Biak, M. Basri, S. Mamat, Colloidal stability and rheology of jatropha oil-based waterborne polyurethane (JPU) dispersion, Prog. Org. Coating 125 (2018) 348–357, https://doi.org/10.1016/j.porgcoat.2018.09.018.
- [51] Y. Shen, C.C. An, J.J. Jiang, B.N. Huang, N.J. Li, C.J. Sun, C. Wang, S.S. Zhan, X. Y. Li, F. Gao, X. Zhao, H.X. Cui, R. Gooneratne, Y. Wang, Temperature-dependent nanogel for pesticide smart delivery with improved foliar dispersion and bioactivity for efficient control of multiple pests, ACS Nano 16 (2022) 20622–20632, https://doi.org/10.1021/acsnano.2c07517.
- [52] J. Wang, Z.B. Tu, M.Q. Zhang, T.R. Ren, N. Chen, B. Zhang, PEGylated strategy for new polyurethane construction and its effects in improving the dispersion stability of tebuconazole suspension concentrate, Colloid Surfaces A 645 (2022) 128847, https://doi.org/10.1016/j.colsurfa.2022.128847.
- [53] C.W. He, Y.F. Xu, M. Ling, X. Huang, Z. Zhou, High internal phase emulsions stabilized by walnut protein amyloid-like aggregates and their application in food 3D printing, Food Hydrocolloid. 147 (2024) 109444, https://doi.org/10.1016/j. foodhyd.2023.109444.
- [54] D.L. Reichard, A system to measure viscosities of spray mixtures at high shear rates, Pest Sci. 47 (1996) 137–143, https://doi.org/10.1002/(SICI)1096-9063 (199606)47:2<137:AID-PS408>3.0.CO;2-M.
- [55] Y.Y. Song, F. Zhu, C. Cao, L.D. Cao, F.M. Li, P.Y. Zhao, Q.L. Huang, Reducing pesticide spraying drift by folate/Zn²⁺ supramolecular hydrogels, Pest Manag. Sci. 77 (2021) 5278–5285, https://doi.org/10.1002/ps.6570.
- [56] J. Feng, Y. Ma, Z. Chen, Q. Liu, J. Yang, Y. Gao, W. Chen, K. Qian, W. Yang, Development and characterization of pyriproxyfen-loaded nanoemulsion for housefly control: improving activity, reducing toxicity, and protecting ecological environment, ACS Sustain. Chem. Eng. 9 (2021) 4988–4999, https://doi.org/ 10.1021/acssuschemeng.0c08105.
- [57] L. Zhang, J. Wang, Y. Fan, Y. Wang, Coacervate-enhanced deposition of sprayed pesticide on hydrophobic/superhydrophobic abaxial leaf surfaces, Adv. Sci. 10 (2023) 2300270, https://doi.org/10.1002/advs.202300270.
- [58] Y.T. Xiao, C.H. Wu, S.S. Feng, M.Y. Chen, H.C. Cao, K. Chen, L. Zhou, Q.X. Yin, Green and efficient delivery of pesticides throughout their life cycle via cooperative solid and solution self-assembly, Chem. Eng. J. 475 (2023) 146037, https://doi. org/10.1016/j.cei.2023.146037.
- [59] Z.L. Luo, Y. Lia, C. Duan, B.B. Wang, Fabrication of a superhydrophobic mesh based on PDMS/SiO₂ nanoparticles/PVDF microparticles/KH-550 by one-step dipcoating method, RSC Adv. 8 (2018) 16251–16259, https://doi.org/10.1039/ CSPA033620.
- [60] Z.Q. Yuan, Y.F. Wu, J.X. Zeng, X.Y. Li, K.R. Zang, H. Zhou, Modified nano-SiO₂/PU hydrophobic composite film prepared through in-situ coupling by KH550 for oilwater separation, Environ. Sci. Pollut. R. 30 (2023) 52958–52968, https://doi.org/10.1007/s11356-023-25900-1.
- [61] S.H. Lu, B. Liang, J.L. Hu, Y.N. Liu, F. Yang, J. Liu, Multidimensional response of dopamine nano-system for on-demand fungicides delivery: reduced toxicity and synergistic antibacterial effects, Chem. Eng. J. 482 (2024) 148990, https://doi. org/10.1016/j.cej.2024.148990.